Molecular Dynamics Simulations of *p*-Sulfonatocalix[4]arene Complexes with Inorganic and Organic Cations in Water: A Structural and Thermodynamic Study

A. Mendes, C. Bonal, N. Morel-Desrosiers, J. P. Morel, and P. Malfreyt*

Laboratoire de Thermodynamique des Solutions et des Polymères, UMR CNRS 6003, Université Blaise Pascal, 24 avenue des Landais, 63177 Aubière Cedex, France

Received: October 17, 2001; In Final Form: January 31, 2002

We report results of simulations of association between *p*-sulfonatocalix[4]arene and inorganic (rare-earth metal cations) and organic cations (a series of quaternary ammonium cations) in aqueous solution. Our main goals were to obtain structural features for these complexes in aqueous solution and to study the role of water on the cation binding by the *p*-sulfonatocalix[4]arene. The MD calculations show that the organic and inorganic cations bind in very different modes. The lanthanide cations are located outside the cavity of the calixarene forming an outer-sphere complex, while for the organic cations, the quaternary ammonium cation is included into the cavity of the calixarene. In fact, the Me_4N^+ cation penetrates deeply into the cavity. As concerns the Et_4N^+ cation, one of the alkyl chain is close to the center of mass of the calixarene, whereas two other alkyl chains are located near the border of the cavity. In the case of Pr_4N^+ cation, only one propyl chain is inside the cavity, while the others are outside the cavity of the calixarene. Additional simulations have been carried out using two different free energy perturbation formalisms to calculate differences in Gibbs free energies of complexation of lanthanide complexes. These simulations are consistent with the thermodynamic properties of association obtained recently by microcalorimetry, and the calculated differences in Gibbs free energies of complexation are in excellent agreement with the experimental ones.

1. Introduction

Calixarenes[1,2] are macrocyclic host molecules built from phenolic units which can bind a variety of guests. Studies of the water-soluble *p*-sulfonatocalix[4]arene (Figure 1) have generated interest owing the similarities to biological function,[3,4] enzyme mimicry,[5] and clay structure.[6,7,8]

We previously reported an experimental study of the association of various inorganic and organic cations with *p*-sulfonatocalix[4]arene in water.[9,10] For each system the thermodynamic parameters of association were determined by microcalorimetry[9] in order to characterize further the driving forces (electrostatic forces, van der Waals forces, or hydrophobic effects ...) involved in the complexation by water-soluble calixarenes. The electrostatic attraction between *p*-sulfonatocalix[4]arene and various rare-earth metal cations (La^{3+}, Nd^{3+}, Sm^{3+}, Eu^{3+}, Gd^{3+}, Dy^{3+}, Yb^{3+}) in an acidic solution (pH 2) were first studied. The binding of a series of quaternary ammonium cations (Me_4N^+, Et_4N^+, Pr_4N^+, Bu_4N^+) was also investigated at pH 2. All the phenolic hydroxy groups of the *p*-sulfonatocalix[4]arene are protonated at pH 2, according to the pK_a values.[11−13] Consequently, the macrocycle is charged −4 due to the four sulfonate groups located on the upper rim of the calixarene. In all cases, the results were consistent with the formation of 1:1 complexes. With the lanthanide cations, the complexation is entropy-driven, whereas the process is essentially enthalpy-driven for the tetraalkylammonium cations.

No direct evidence was nevertheless obtained about the structures and the nature (outer-sphere, solvent-separated or inner-sphere, contact ion pair) of the lanthanide complexes in solution. With lanthanide cations, the electrostatic interactions play a major role in the association process. The lanthanide cations are probably located near the negatively charged sulfonate group (outside the cavity of the calixarene). For the organic cations, it is known that there is an inclusion of the alkylammonium cation into the cavity of the calixarene.[3] The major contribution to the enthalpy of complexation of these species probably comes from the van der Waals interaction associated with the inclusion of the alkyl chains with some contributions of hydrophobic interactions. The solid-state structure of the *p*-sulfonatocalix[4]arene complex with tetramethylammonium ions was reported by Atwood et al.[14] Their results showed that the embedded tetramethylammonium ions display

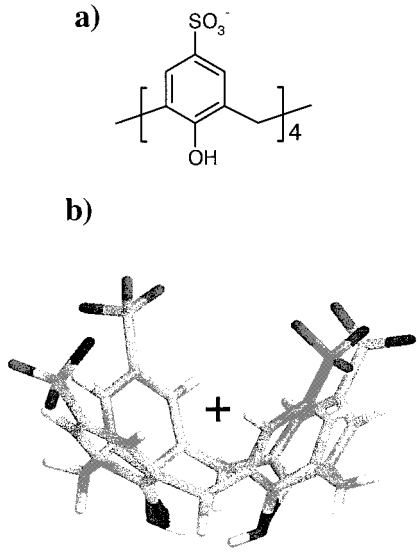

Figure 1. (a) *p*-Sulfonatocalix[4]arene; (b) skeleton scheme of free calixarene anion showing the position of the center of mass represented by (+).

* Corresponding author: patrice.malfreyt@univ-bpclermont.fr.

10.1021/jp013848y CCC: $22.00
Published on Web 04/05/2002

one methyl group deep within the cavity and three at the upper rim. Unfortunately, the relevance of solid-state structures for representing structures in solution is questionable.

Understanding in detail the thermodynamic properties of association requires knowledge of the precise structure of these complexes in solution. As far as we know, no molecular simulations on these *p*-sulfonatocalix[4]arene complexes has been reported. This led our group to perform molecular simulations to get information that make interpretation of these experimental results easier. Our main goals are to obtain structural information in these complexes in aqueous solution and to study the role of water on the cation binding by the *p*-sulfonatocalix[4]arene. Additional simulations have been carried out using free energy perturbation methods to calculate relative binding affinities of lanthanide complexes.

Merbach et al.[15] have developed lanthanide parameters with a three-body potential function, taking into account the mean polarization of water molecules in the first hydration shell. Unfortunately, the development of realistic polarizable models for water must be consistent with the force-field parameters currently available. This type of work is in progress although some authors continue to explore and develop new rigid models for water with effective pair potentials.[16] In addition, taking into account polarization or charge-transfer effects makes MD simulations of such complexes a cumbersome, time-consuming, and costly tool. Furthermore, these models must be calibrated over a large number of simple systems before the studies of more sophisticated systems. In view of the preceding, we use nonpolarizable potentials as the majority of molecular simulations already published over this kind of complex.

The remainder of this paper is arranged as follows. Section 2 contains a description of the intramolecular and intermolecular interactions and the computational techniques we have employed in our simulations. In section 3, we present the results of the simulations and relate these to experimental data. Finally, in section 4, we draw the main conclusions from our work.

2. Simulations

2.1. Potential Model. The *p*-sulfonatocalix[4]arene molecule is modeled by the all-atom version of the Cornell force field AMBER.[17] The general potential function is of the form

$$U = \sum_{\text{bonds}} k_b(r - r_o)^2 + \sum_{\text{angles}} k_\theta (\theta - \theta_o)^2 + \sum_{\text{dihedrals}} k_\phi[1 + \cos(n\phi + \delta)] + \sum_{i=1}^{N-1}\sum_{j>i}^{N}\left\{4\epsilon_{ij}\left[\left(\frac{\sigma_{ij}}{r_{ij}}\right)^{12} - \left(\frac{\sigma_{ij}}{r_{ij}}\right)^{6}\right] + \frac{q_i q_j}{4\pi\epsilon_0 r_{ij}}\right\} \quad (1)$$

where the first three terms represent the bond, angle, and torsion interactions. The C−H and O−H covalent bonds are kept of fixed length by use of the SHAKE algorithm[18] and the aromatic rings are kept planar using six improper torsional potentials. In the AMBER force field, the nonbonded interactions between atoms separated by exactly three bonds (1−4 van der Waals interactions) are reduced by a factor of 0.5 following ref 17. The bond, bond angles, dihedral angles, and LJ parameters for the sulfonate group are taken from ref 19. The Lennard-Jones parameters for the trivalent lanthanides ions La^{3+}, Eu^{3+}, and Yb^{3+} have been determined to reproduce the free energy of hydration in water by Veggel et al.[20] More recently, another set of parameters for La^{3+}, Eu^{3+}, and Lu^{3+} has been published.[21] We decide to use the LJ parameters determined by Veggel et al.[20] because the parametrized series corresponds better to that studied by microcalorimetry.[9] The Lennard-Jones potential parameters for the interactions between unlike atoms are calculated by using the Lorentz−Berthelot mixing rules. The charges are computed using the AM1 Hamiltonian on the crystal structure.[22] The water molecules are represented with the TIP3P model.[23]

2.2. Computational Details. The system consists of one *p*-sulfonatocalix[4]arene molecule with a lanthanide or organic cation and 900 water molecules. Depending on the studied complex, one or more Cl^- anions are added to ensure the electroneutrality in the box. The Cl^- anions are located in such a way that the distances $Cl^-\cdots La^{3+}$, $Cl^-\cdots Cl^-$, and $Cl^-\cdots Cal^{4-}$ are roughly equal to the cutoff, implying no interaction between these species. The calixarene is immersed at the center of a cubic solvent box. For the lanthanide complex, the starting conformation is built by locating the naked La^{3+} close to the sulfonate groups. For the organic cation complexes, the center of mass of the tetraalkylammonium cations is initially placed in order that the alkyl groups do not penetrate into the cavity. The conformation of the calixarene is minimized by performing a zero temperature MD simulation to allow a relaxation of the conformation. The solvent molecules are added with random orientations, avoiding direct overlap with them. The periodic boundary conditions are applied in all the three dimensions. The Ewald summation technique is applied for the treatment of the long-range electrostatic interactions[24] with the range of the real space interaction controlled by the convergence parameter $\alpha = 0.265$ within a relative error of 10^{-6}. The reciprocal space summation is performed by using $k_{max} = \{10 \text{ x } 10 \text{ x } 10\}$. The equations of motions are integrated using the Verlet leapfrog algorithm scheme in the NpT ensemble ($p = 1$ atm and $T = 298$ K) with a 2 fs time step. We used the Berendsen algorithm[25] with coupling constants 0.1 ps (temperature) and 0.5 ps (pressure). We used the multiple time step algorithm[26] in conjunction with the Verlet neighbor list. The interval for computing the secondary force is taken equal to five steps with a large cutoff ($r_c = 12$ Å), whereas the primary force is calculated every time step within a cutoff of 8 Å. The Verlet list sphere radius is fixed to 14 Å. Using this set of parameters, we have checked that the total energy of our systems is well conserved with deviations less than 0.3%. A typical run consisted of 200 ps of equilibration followed by a production phase of an additional 500 ps. The structural and thermodynamic quantities are calculated over 25 000 configurations saved during the run. All the simulations are performed by using the DL_POLY_MD package,[27] each simulation required ca. 2 weeks of CPU time on a Pentium III workstation.

2.3. Free Energy Calculations. The difference in Gibbs free energies ΔG between molecular systems A and B are calculated with the free energy perturbation (FEP)[28,29] and the thermodynamic integration (TI)[29−31] methods. In the FEP approach, the computation of free energy difference between two states A and B in the NpT ensemble is divided in a N_w number of intermediate contiguous states or windows defined by a coupling constant λ

$$\Delta G = G_B - G_A = \sum_{i=1}^{N_w}\Delta G_i = \sum_{\lambda=0}^{1} -RT \ln\left\langle \frac{V \exp\left[-\frac{(H(r;\lambda \pm \Delta\lambda) - H(r;\lambda))}{RT}\right]}{\langle V\rangle}\right\rangle \quad (2)$$

where $H(r, \lambda)$ is the classical Hamiltonian corresponding to the state λ and depending only on the atomic coordinate set r. R is the molar gas constant, T is the absolute temperature, and V the volume of the system. $\langle\ \rangle$ denotes an isothermal−isobaric ensemble average. In our FEP simulations, the perturbations are performed in both directions ("double-wide sampling") with ($N_w = 21$; $\Delta\lambda = 0.05$) windows over the entire simulation. The difference between the forward and backward simulations gives an estimation of the statistical uncertainty of the calculations.

The thermodynamic integration method expresses the change in free energy as the following integral

$$\Delta G = \int_0^1 \left\langle \frac{\partial H(r;\lambda)}{\partial \lambda} \right\rangle \mathrm{d}\lambda \tag{3}$$

In this paper, we use the perturbation formalism to compute the derivation of the Hamiltonian wih respect to λ and this technique is commonly referred as the finite difference integration thermodynamic (FDTI) method. In this case, the derivative of the Hamiltonian can be approximated with a finite difference:

$$\left\langle \frac{\partial H(r;\lambda)}{\partial \lambda} \right\rangle = \frac{\partial G(\lambda)}{\partial \lambda} \simeq \frac{\Delta G(\lambda)}{\delta \lambda} = -\frac{RT}{\delta\lambda} \ln \left\langle \frac{V \exp\left[-\frac{(H(r;\lambda \pm \delta\lambda) - H(r;\lambda))}{RT}\right]}{\langle V \rangle} \right\rangle \tag{4}$$

In our work, $\delta\lambda$ is taken sufficiently small ($\delta\lambda = 0.001$) to avoid hysteresis between calculations carried out from state λ to state $\lambda + \delta\lambda$ and that from state λ to state $\lambda - \delta\lambda$ and to attain a proper convergence leading to energy differences smaller than 1 kJ mol^{-1}. Simulations in the forward ($+\delta\lambda$) and the reverse ($-\delta\lambda$) directions provide the average value of the derivative with a measure of the statistical uncertainty. Then, the final integration over λ (eq 3) is carried out by an trapezoidal algorithm to obtain the free energy difference.

The variations of the Hamiltonians $H(r; \lambda)$ are calculated by using a linear combination of the LJ parameters (σ, ϵ) of the initial state A ($\lambda = 0$) and final state B ($\lambda = 1$) using the following mixing rules:

$$\epsilon_{ij} = \lambda\left(\sqrt{(\epsilon_{ii}\epsilon_{jj})}\right)_{(\lambda=1)} + (1-\lambda)\left(\sqrt{(\epsilon_{ii}\epsilon_{jj})}\right)_{(\lambda=0)} \tag{5}$$

$$\sigma_{ij} = \lambda\left(\frac{\sigma_{ii}+\sigma_{jj}}{2}\right)_{(\lambda=1)} + (1-\lambda)\left(\frac{\sigma_{ii}+\sigma_{jj}}{2}\right)_{(\lambda=0)} \tag{6}$$

where i and j represent atom types.

Each window consists of 5 ps of equilibration followed by 10 ps of acquisition corresponding to 5000 configurations for the average calculations. The total time per FEP or FDTI run is 315 ps.

2.4. Molecular Shape Parameters. The shape of the macrocyclic molecule can be also estimated from the inertia tensor **S**

$$S_{\alpha\beta} = \frac{\sum_{i=1}^{N_c} m_i (r_i^{\alpha} - r_{\mathrm{com}}{}^{\alpha})(r_i^{\beta} - r_{\mathrm{com}}{}^{\beta})}{\sum_{i=1}^{N_c} m_i} \tag{7}$$

where α and β are x, y, or z, m_i is the mass of the ith atom, and r_i^{α} is the α component of the position vector of atom i. The subscript "com" refers to the center of mass of the *p*-sulfonatocalix[4]arene molecule and N_c is the total number of atomic sites. Diagonalization of S results in three eigenvalues γ, which sum the mean-squared radius of gyration $\langle R_g^2 \rangle$ and the largest of which corresponds to an eigenvalue vector representing the long axis of the macrocycle. A useful descriptor of anisometry is the asphericity[32] order parameter, A, defined as

$$A = \frac{\sum_{i>j} (\gamma_i - \gamma_j)^2}{2(\sum_{i=1}^{3} \gamma_i)^2} \tag{8}$$

A measures the deviation from a spherical form. If A tends to zero, the macrocycle adopts a spherical conformation, while A tends to 1 as the cycle becomes a thin rod.

2.5. Dynamical Properties of Water around the Calixarene. The mean residence time reflects the decay of the hydration shell of an ion or a molecule in the course of time. The residence time has been calculated from the correlation function $r(t)$ defined as[33,34]

$$r(t) = \frac{\langle P_j(t, t_i; t^*)_{i,j} \rangle_{i,j}}{\langle P_j(0, t_i; t^*) \rangle_{i,j}} \tag{9}$$

This function gives a probability for a water molecule in the hydrated shell to lie there during time t. The parameter t^* is introduced to take into account molecules which leave the coordination shell temporarily and return back without properly entering the bulk solution. As in previous works,[35,36] we have set t^* equal to 2 ps. The $P_j(t, t_i; t^*)$ takes the value 1 if water molecule j lies within the coordination shell of the cation at both times t_i and $t_i + t$, and in the interim it does not leave the coordination shell for any continuous period longer than t^*. The time correlation function $r(t)$ can be fitted to a second-order exponential decay:[37]

$$r(t) = A_1 \exp\left(-\frac{t}{\tau_1}\right) + A_2 \exp\left(-\frac{t}{\tau_2}\right) \tag{10}$$

In eq 10, the first term corresponds to an escape of the solvent molecules located close to the border of the considered shell at a time of about τ_1 ps. The second term describes a persistence of the shell around the considered species, and τ_2 corresponds to the residence time of the solvent molecules. Roughly, the fitted parameters A_1 and A_2 can be interpreted as the percentage of the solvent molecules involved in both processes.

3. Results and Discussion

The radial distribution functions for La^{3+} and the oxygen and hydrogen atoms of water molecules are shown in Figure 2 for the free cation and for the cation in the complex. We check that the distribution functions calculated in the complex match very well with those calculated for the free ions, except for a slight difference in the height of the first peak in the $La^{3+}\cdots O$ distribution function. The average coordination numbers of water molecules in the first hydration shell and the mean distances $La^{3+}\cdots O$ are equal to 10.0 ± 0.2 and 2.71 ± 0.02 Å for the free cations and 10.6 ± 0.9 and 2.74 ± 0.04 Å for the cation in the complex. In the second hydration shell, the coordination number of water is 20.1 ± 1.8 for the free cation and 17.7 ± 2.5 for the complex. The mean distance between the La^{3+} cation and the oxygen of the water molecule in the second hydration shell is strictly identical for the free cation and for the complex

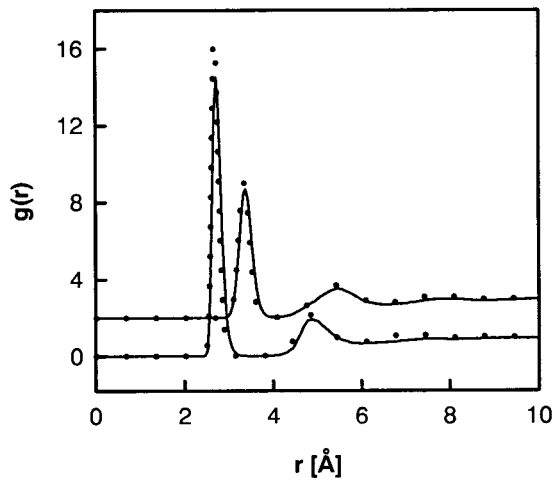

Figure 2. Compted $g_{La^{3+}\cdots OH_2}$ and $g_{La^{3+}\cdots H_2O}$ radial distribution functions for the free cation La^{3+} (···) and for the cation La^{3+} in the complex $(Cal, La)^-$ (—) at 298 K in TIP3P water model from MD simulations. The computed $g_{La^{3+}\cdots H_2O}$ distribution functions are offset by 2 Å for clarity.

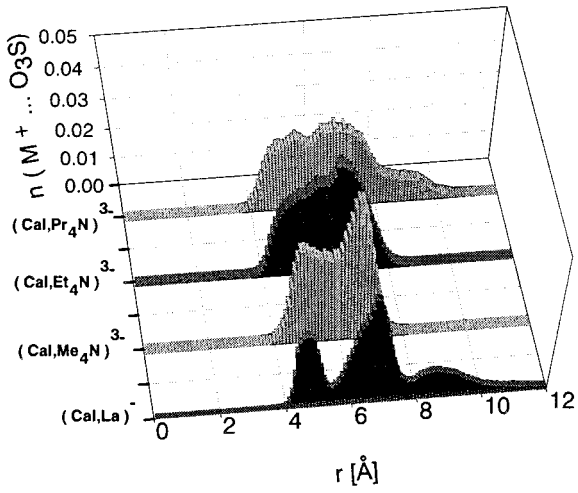

Figure 3. Distributions of the distances between the La^{3+} cation or the nitrogen cation of tetraalkylammonium cations and the oxygen atoms of the sulfonate groups versus the studied complexes.

$(5.0 \pm 0.1$ Å). These first results underline that the first hydration shell is not perturbated by the presence of the *p*-sulfonatocalix-[4]arene, unlike the second hydration shell. The distance between the center of mass of the calixarene and La^{3+} (5.9 ± 1.2 Å) in conjunction with the unchanged first hydration shell shows that La^{3+} is not directly bonded to the ligand. This can also be shown in the distribution of the distances between La^{3+} and the oxygens of sulfonate groups varying from 4 to 12 Å (Figure 3). The first peak of this broad distribution is located at 5 Å and corresponds to three oxygens of sulfonate groups replacing the released water molecules of the second hydration shell of La^{3+}. The MD simulations performed in vacuo from the same starting conformation show that the first peak of the distribution between La^{3+} and the oxygens of the sulfonate groups is shifted at 2.4 Å. In the gaseous phase, La^{3+} is close to the sulfonate groups, whereas in water it is separated by its first hydration shell. The *p*-sulfonatocalix[4]arene is therefore located in the outer coordination sphere of the metal ion forming an outer-sphere complex in which La^{3+} preserves a certain mobility.

In Table 1 are reported the three eigenvalues of the inertia tensor for the free ligand and for the complex with La^{3+}. The calculation of the asphericity coefficient (A) from eq 8 shows,

TABLE 1[a]

	$(Cal)^{4-}$	$(Cal, La)^{1-}$	$(Cal, Me_4N)^{3-}$	$(Cal, Et_4N)^{3-}$	$(Cal, Pr_4N)^{3-}$
$\langle\gamma_1\rangle$	12.7_{11}	11.7_{15}	11.7_6	11.5_6	12.3_7
$\langle\gamma_2\rangle$	9.3_{11}	8.6_9	10.4_6	10.2_5	9.9_7
$\langle\gamma_3\rangle$	4.1_3	4.1_2	3.8_3	3.7_1	3.6_2
$\langle R_g^2\rangle$	26.1_{11}	24.4_8	25.9_7	25.5_5	25.9_6
$\langle A\rangle$	0.09_2	0.08_3	0.08_1	0.08_1	0.09_1
M···com		5.9_{12}	2.2_2	3.4_2	4.6_2

[a] $\langle\gamma_1\rangle$, $\langle\gamma_2\rangle$, and $\langle\gamma_3\rangle$ represent the mean length (Å) of the longest, intermediate, and smallest axis of the calixarene, respectively. R_g^2 is the mean squared radius of gyration (Å^2) of the macrocyle and $\langle A\rangle$ is the mean value of the asphericity parameter defined as in eq 8. The average distance M···com represents the distance between La^{3+} and the center of mass of calixarene in the $(Cal, La)^-$ complex. For the organic complexes, this distance is calculated from the nitrogen atom of the tetraalkylammonium cations. The subscript indicates the accuracy of the last decimal(s). The number 9.3_{11} means 9.3 ± 1.1.

for all the structures studied in this work, that the global conformation is quite spherical with a value of A close to 0. Accordingly, we may compare the structure of the calixarene to a sphere with a radius equal to the root-mean-square radius of gyration ($R_g \approx 5$ Å). We note no significant change on the three eigenvalues between the free ligand and the complex with La^{3+} suggesting no important conformational changes. The comparison of these values with those calculated in the complexes with tetraalkylammonium cations shows significant changes in the intermediate and smallest eigenvalues γ_2 and γ_3. Actually, γ_2 increases with the organic cations, whereas γ_3 decreases. We observe also a slight decrease in the γ_2 and γ_3 values from Me_4N^+ to Pr_4N^+ cations. These results suggest that the complexes formed with organic ions adopt conformations in which the cavity of the calixarene is more open. The mean distances between the nitrogen atoms of the tetraalkylammonium ions and the center of mass of calixarene are included in Table 1. For the tetraalkylammonium ions, these values increase from 2.2 to 4.6 Å, whereas this value is equal to 5.9 Å for the (Cal, La)$^{-1}$ complex. According to these distances, there is inclusion of R_4N^+ cation into the cavity of the calixarene. To show this insertion, we have plotted the distributions of each carbon atom located at the ends of the alkyl chains for the tetraalkylammonium cations (Figure 4). In this figure, are displayed the positions of the center of mass of calixarene and the root-mean-square radius of gyration. We distinguish two peaks for the Me_4N^+ cation and three peaks for the Et_4N^+ and Pr_4N^+ cations. For all the organic cations studied here, the first peak is located at the same position from the center of mass of the calixarene, indicating the insertion of one alkyl chain into the cavity. As a function of the organic complex, we obtain the second peak inside or outside the cavity. In the $(Cal, Me_4N)^{3-}$ complex, one methyl is located near the center of mass of the calixarene (first peak) and the second peak can be attibuted to the three remaining CH_3 groups located on a sphere at the same distance from the center of mass of calixarene. This singularity of the Me_4N^+ cation is due to its tetrahedral geometry. We deduce that the Me_4N^+ cation penetrates deeply into the cavity. This result is in agreement with the solid structure of the *p*-sulfonatocalix[4]arene complex with tetramethylammonium ion determined by Atwood et al.[14] Because of the increase in the length of the alkyl chains, there is no more tetrahedral geometry for the ends of the alkyl chains for Et_4N^+ and Pr_4N^+ cations. We obtain then three peaks in the distributions of the CH_3 end groups. As concerns, the $(Cal, Et_4N)^{3-}$ complex, the second peak is displaced toward the border of the cavity. The height of this peak indicates the presence of two methyl groups close to the

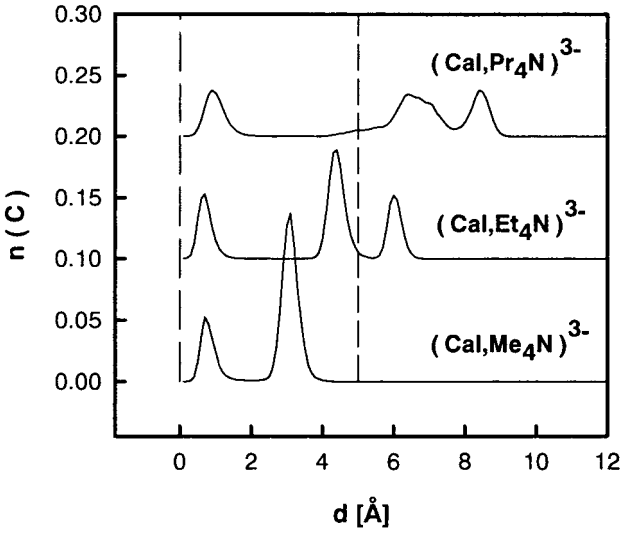

Figure 4. Distributions of the distance between each carbon atom located at the ends of the alkyl chains and the center of mass of the calixarene in the (Cal, Me_4N)$^{3-}$, (Cal, Et_4N)$^{3-}$, and (Cal, Pr_4N)$^{3-}$ complexes. For clarity, the distributions in (Cal, Et_4N)$^{3-}$ and (Cal, Pr_4N)$^{3-}$ complexes are vertically shifted by 0.1 unit. The position of the center of mass and of the radius of gyration are represented by two dashed lines at $d = 0$ and $d = 5$.

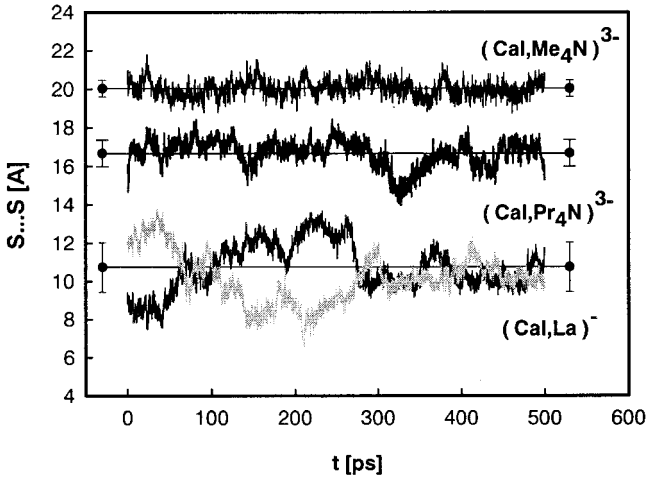

Figure 5. Distances S···S (Å) between two opposite sulfur atoms located at the two ends of the calixarene in the (Cal, La)$^{-}$ complex. The gray curve represents the distance between the two others opposite sulfur atoms. The trajectories of the S···S distances are offset by 5 Å for (Cal, Pr_4N)$^{3-}$ and by 9 Å for (Cal, Me_4N)$^{3-}$. The straight lines correspond to the average S···S distance and the error bars represent rms fluctuations.

border of the cavity. On the other hand, the examination of the distribution of the Pr_4N^+ cation shows two peaks superiors to R_g and indicates that three propyl chains are outside the cavity of the calixarene. Moreover, compared to Me_4N^+ and Et_4N^+, the distribution between the N^+ cation and the O atoms of the sulfonate groups (Figure 3) indicates a profile of the same broadness for the (Cal, La)$^{1-}$ and (Cal, Pr_4N)$^{3-}$ complexes, in agreement with the fact that the inclusion of only one propyl chain implies a certain flexibility of the calixarene and a mobility of the cation.

As concerns the flexibility of the calixarene, we have reported the trajectories of the distances between two opposite sulfurs located at the two ends of the macrocycle in Figure 5. In the case of the La^{3+} complex, the synchronous exchange between the two trajectories shows that the macrocycle oscillates between two symmetrical conformations and underlines the conformational flexibility of calixarene in this complex. The trajectories calculated in the (Cal, Me_4N)$^{3-}$ complex are constant within the standard deviation and indicate a rigid conformation due to the deep insertion of the Me_4N^+ group into the cavity. With the Pr_4N^+ cation, we have an intermediate situation in which the insertion of one chain reduces only partially the flexibility of the calixarene.

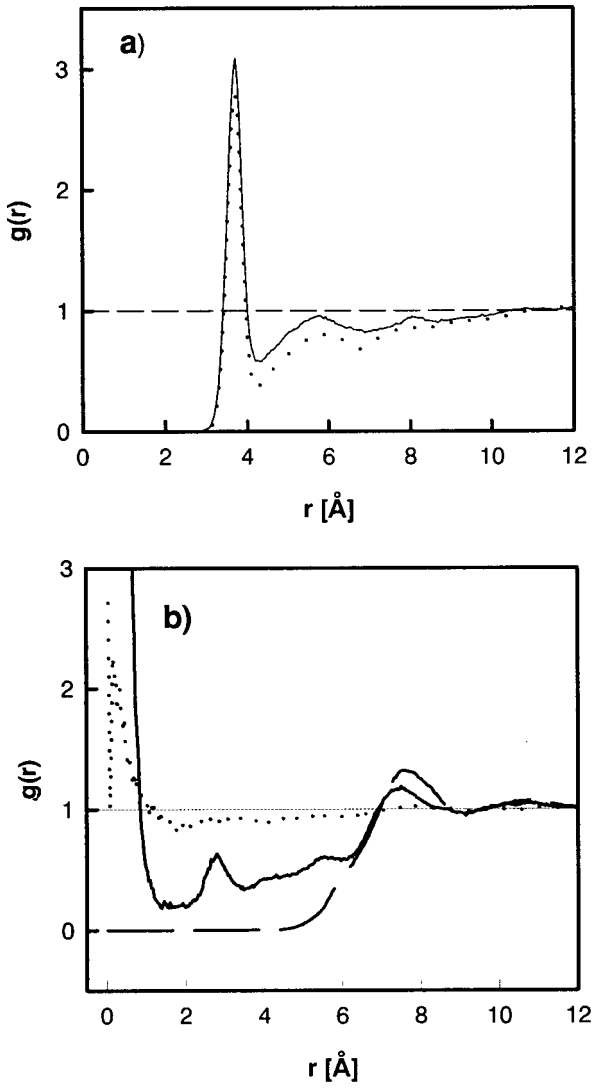

Figure 6. (a) Computed $g_{S\cdots OH_2}$ radial distribution functions between the sulfur of sulfonate groups and the water molecules in the (Cal, La)$^{-}$ (—) and (Cal, Pr_4N)$^{3-}$ (···) complexes; (b) $g_{com\cdots OH_2}$ radial distribution functions between the center of mass of calixarene and the water molecules in the free anion (···), in the (Cal, La)$^{-}$ complex (—), and in the (Cal, Et_4N)$^{3-}$ complex (---).

TABLE 2[a]

	(Cal)$^{4-}$	(Cal, La)$^{1-}$	(Cal, Me_4N)$^{3-}$	(Cal, Et_4N)$^{3-}$	(Cal, Pr_4N)$^{3-}$
$n_{(H_2O,\ SO_3^-)}$	8.6	8.8	7.9	7.2	7.5
τ_2	17.4	21.1	20.0	22.2	21.9
$n_{(H_2O,\ cavity)}$	8.1	4.0	0.0	0.0	0.0
τ_2	31.6	31.0			

[a] $n_{(H_2O,\ SO_3^-)}$ and $n_{(H_2O,\ cavity)}$ are the average number of water molecules located in the first hydration shell of the sulfonate groups and inside the cavity of the calixarene, respectively. τ_2 is the corresponding residence time resulting from the fit of the time correlation function to an exponential decay defined in eq 9.

The radial distribution functions between the sulfur atom of the sulfonate groups and the oxygen of the water molecules

TABLE 3: Differences in Computed Gibbs Free Energy (kJ mol^{-1}) between the $La^{3+}\cdots Eu^{3+}$ and $La^{3+}\cdots Yb^{3+}$ Mutations for the Free and Complexed Lanthanides Cations[a]

	ΔG_3		ΔG_3	ΔG_4		$\Delta\Delta G_c$		$\Delta\Delta G_c$
	FEP	FDTI	MC	FEP	FDTI	FEP	FDTI	exptl
$La^{3+}\cdots Eu^{3+}$	-238.5_5	-238.5_5	-232.7_{23}	-237.2_5	-237.2_5	-1.3_5	-1.3_5	-2.2
$La^{3+}\cdots Yb^{3+}$	-433.0_9	-432.8_5	-417.8_{61}	-429.0_{15}	-429.0_{15}	-4.0_{15}	-3.9_5	-2.3

[a] The relative free energies of hydration ΔG_3 calculated by using the FEP method with Monte Carlo simulations[20] are also reported. The relative experimental free energies of complexation[9] are given for comparison. The subscript indicates precision as in Table 1.

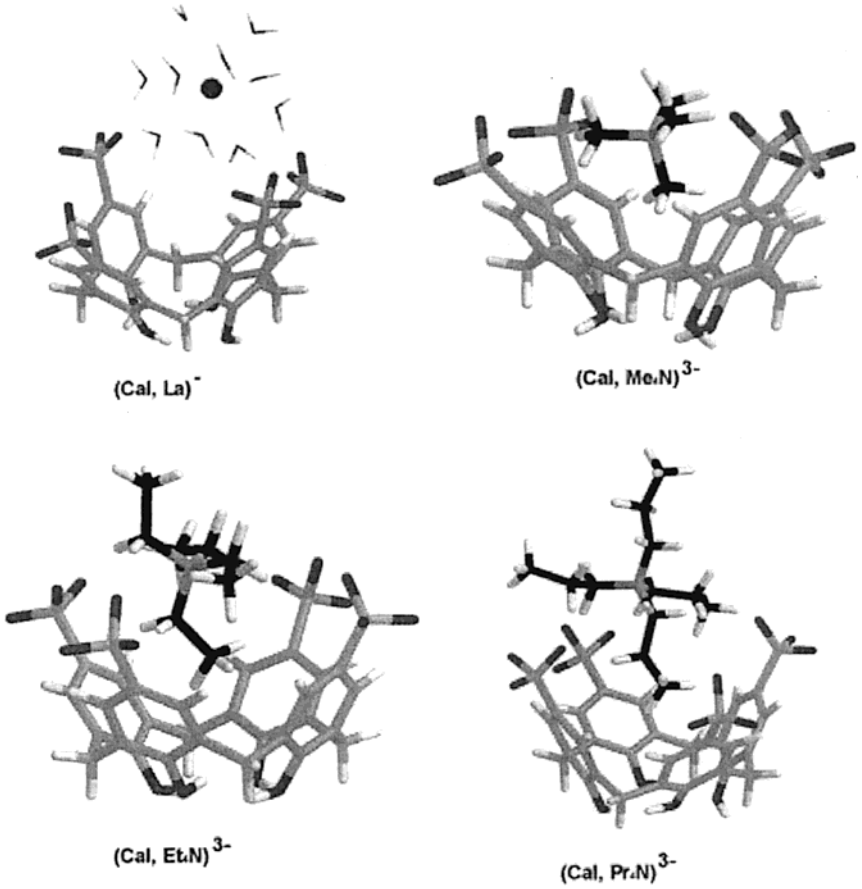

Figure 7. Snapshots from MD simulations. In the (Cal, La)$^-$ complex are included the water molecules located in the first hydration shell of La^{3+}.

are displayed in Figure 6a for the (Cal, La)$^-$ complex and (Cal, $Pr_4N)^{3-}$ complexes. We note no important change between these two curves. The integration of the first peak yields the mean number of water molecules in the first hydration shell (see Table 2). We find no desolvation of the sulfonate groups of calixarene. In Figure 6b, the radial distribution functions between the center of mass of calixarene and the water molecules are also plotted. We observe dramatic changes with the distributions involving organic cations inside the cavity. In fact, with organic cations, the distribution is constant and equal to 0 until 5 Å. The mean number of water molecules reported in Table 3 corresponds to the integration of the distribution function from the center of mass to 4 Å. This distance is taken smaller than the root square of the radius of gyration to ensure that we are really inside the cavity. The number of water molecules in the cavity decreases from 8.1 for the free ligand to 4.0 for the (Cal, La)$^{1-}$ complex, and we obtain a total desolvation with the organic ions. All the structural features of the studied complexes can be visualized in Figure 7 through instantaneous conformations resulted from our calculations.

Figure 8a presents the residence time correlation functions for the water molecules in the second hydration shell of both the free La^{3+} cation and the La^{3+} in the complex. The time correlation functions for the water molecules inside the cavity in the free ligand and in the (Cal, La)$^{1-}$ complex are reported in Figure 8b. We give the time correlation functions for the water molecules in the first hydration shell of the sulfonate groups for the free ligand and the (Cal, La)$^{1-}$ and (Cal, $Pr_4N)^{3-}$ complexes in Figure 8c. The residence time τ_2 results from a fit of the correlation function by an second-order exponential decay. The residence time values are listed in Table 2. The results indicate that the residence time of water molecules in the first hydration shell of the sulfonate groups is of the same order of magnitude for all studied complexes but differs for the free ligand. The higher value of this residence time in the complexes may be explained by the fact that the exchange with solvent molecules in the first hydration shell of the sulfonate group is perturbed and slowed by the presence of the guest molecule. The residence time values of the water molecules in the second hydration shell are equal to 13.8 ps for the free La^{3+} cation and 17.1 ps for the (Cal, La)$^{1-}$ complex. The fact that some of the water molecules in the second hydration of La^{3+} interact with some oxygens of the sulfonate groups implies an increase of the residence time. The residence time of the water molecules inside the cavity is higher and equal to about 31 ps for both the free ligand and the (Cal, La)$^{1-}$ complex. It is worthy

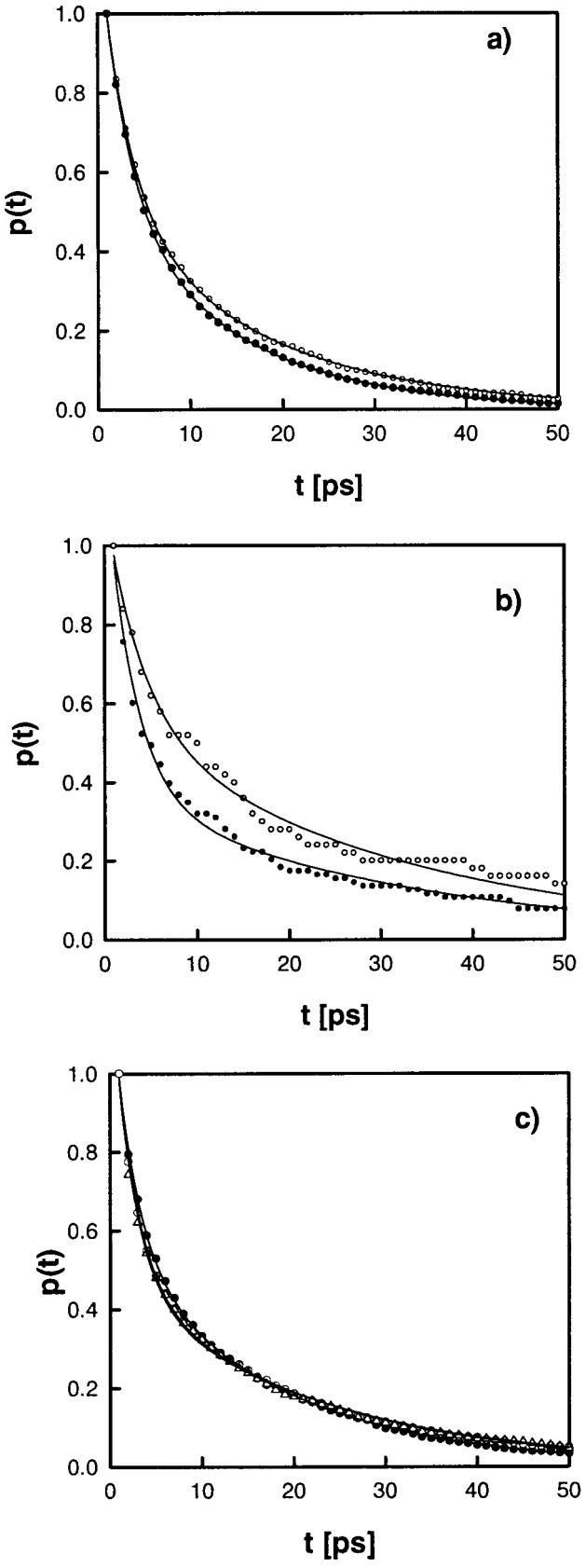

Figure 8. Residence time correlation functions (a) for the water molecules in the second hydration shell of La^{3+} cation free (○) and in the lanthanide complex (●), (b) for the water molecules in the cavity of the free ligand (●), and in the (Cal, La)$^-$ complex (○), (c) for the water molecules in the first hydration shell of sulfonate groups in the free ligand (●), in the (Cal, La)$^-$ complex (○), and in the (Cal, Pr_4N)$^{3-}$ complex (△). The solid lines describe the fitted curves using a second-order exponential decay.

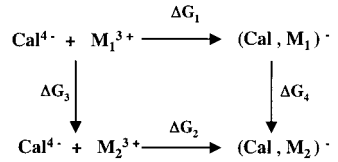

Figure 9. Thermodynamic cycle used to determine the relative Gibbs free energy of complexation $\Delta\Delta G_c$.

of note that the time correlation function calculated in the (Cal, La)$^{1-}$ complex is not as well-defined because of the smaller number of water molecules inside the cavity for the (Cal, La)$^{1-}$. The parameter A_1 is equal to 0.80 for the free ligand and 0.55 for the (Cal, La)$^{1-}$ with a value of τ_1 shorter than about 4 ps. This result means that 80% of water molecules located in the cavity are close to the border and may leave the cavity at a time about 4 ps, whereas this number is equal to 55% for the (Cal, La)$^{1-}$ complex. The number of solvent molecules not leaving the cavity within 0.5 ns simulation time is equal to zero for the free ligand and for the (Cal, La)$^{1-}$ complex, whereas the number of solvent molecules which were found at least once inside the cavity during 0.5 ns is equal to 67 for the free ligand and 33 for the (Cal, La)$^{1-}$ complex. All these results confirm a higher mobility and further exchange for the water molecules inside the cavity of the free ligand, although the average residence time is the same in both cases.

Recently, the thermodynamic parameters characterizing the complexation of the *p*-sulfonatocalix[4]arene by seven rare-earth metals representative of the whole lanthanide series have been determined by microcalorimetry. In all cases, the results showed that the association process is enthalpically unfavored and entropically favored. The positive entropic term was explained by the desolvation of host and guest upon complexation and the consequent release of water molecules. Our MD calculations highlight that the favorable entropic term is due to the partial desolvation of both the cavity of the calixarene and the second hydration of the trivalent cation. For the organic cations, microcalorimetry studies showed that the complexation is driven by a favorable enthalpy and a small change in $T\Delta S$. According to our simulations, the interaction is governed by the inclusion of alkyl groups within the cavity. The complexation of Et_4N^+, which corresponds to the inclusion of the largest number of methylene groups, is characterized by an enthalpy change much more negative than for the other R_4N^+ cations. The small entropy change results from two different contributions: a favorable term due to the total desolvation of the cavity and an unfavorable term due to the insertion of the alkyl chain into the cavity, which implies a loss of conformational flexibility for the calixarene. To reproduce the variations in the free energy of complexation for the complexes involving lanthanide cations, we have performed free energy perturbation simulations.

According to the thermodynamic cycle shown in Figure 9, the difference of the free energies of formation of the (Cal, M_1)$^{1-}$ and (Cal, M_2)$^{1-}$ complexes can be obtained experimentally as $\Delta\Delta G_c = \Delta G_1 - \Delta G_2$ and computationally as $\Delta G_c = \Delta G_3 - \Delta G_4$. ΔG_3 corresponds to the difference in free energies of hydration of the uncomplexed cations, whereas ΔG_4 is calculated by mutation of the complexed M_1^{3+} cation into M_2^{3+} using the same computational procedures as for the free ions. The calculated ΔG_3, ΔG_4, and $\Delta\Delta G_c$ using the two different techniques are given in Table 3. The free energies of hydration ΔG_3 calculated from MC simulations[20] using the FEP method are given in this table. Our calculated ΔG_3 values are slightly more negative than the ones resulting from MC simulations. In fact, the difference between the two sets of computed values

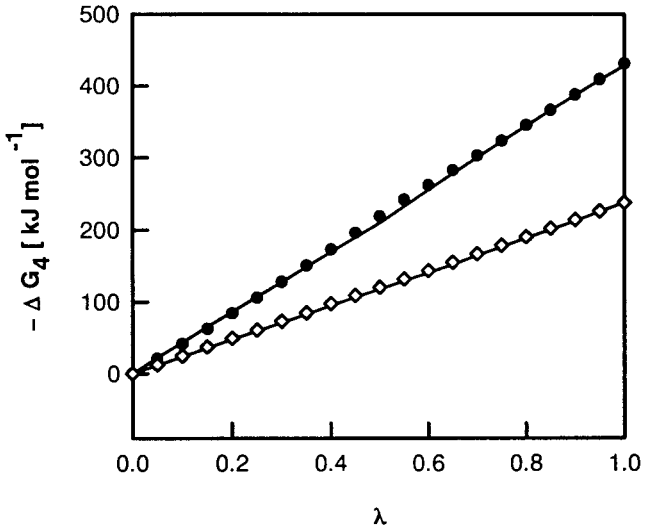

Figure 10. Computed Gibbs free energy changes for the mutation of (Cal, La)$^-$ to (Cal, Eu)$^-$ complexes in forward (—) and reverse (◊) processes and for the mutation of (Cal, La)$^-$ to (Cal, Yb)$^-$ in the forward (—) and reverse (●) directions.

are less than 4%. The MC calculations[20] have been performed with a shifted and truncated potential using a cutoff value of 15 Å. MC creates configurations according to energy criteria, while MD uses forces route. The fact that our configurations have not been generated in the same way (MC or MD) and the small differences in the parameters (cutoff, shifted potential) may explain the slight deviations in the computed free energy of hydration.

The relative experimental Gibbs free energies are also reported. The computed free energy changes ΔG_4 in forward and reverse processes are displayed in Figure 10. The difference in Gibbs free energy between the (Cal, La)$^{1-}$ and (Cal, Eu)$^{1-}$ complexes is predicted with a deviation of less than 1 kJ mol^{-1} with the corresponding experimental value, whereas this difference agrees to within 1.7 kJ mol^{1-} for the (Cal, La)$^{1-}$ and (Cal, Yb)$^{1-}$ complexes. These simulations show an excellent agreement between predicted and experimental values, validating the set of energetic parameters and computational procedures used in this work.

4. Conclusions

We have carried out molecular dynamics simulations of *p*-sulfonatocalix[4]arene with inorganic (rare-earth metal cations) and organic cations (a series of quaternary ammonium cations) in aqueous solution. Results show that La^{3+} is located outside the cavity of the calixarene forming an outer sphere complex. We notice that this cation preserves a certain mobility in the complex. The relative Gibbs free energies of complexation between the (Cal, La)$^-$ and (Cal, Eu)$^-$ complexes and the (Cal, La)$^-$ and (Cal, Yb)$^-$ complexes have been calculated and are in excellent agreement with the corresponding experimental data. This result validates the set of force field parameters used for the ligand and the lanthanide cations.

The association process implies conformational changes with the organic cations. Actually, MD simulations show that the complexes adopt conformations in which the cavity of the calixarene is more open. In fact, there is inclusion of the tetraalkylammonium ammonium cation into the cavity of the calixarene. The Me_4N^+ penetrates deeply into the cavity. As concerns the Et_4N^+ cation, one of the alkyl chains is inside the cavity and two other alkyl chains are close to the border of the cavity. For Pr_4N^+, results show only one propyl chain inside the cavity and the others outside. Accordingly, (Cal, Me_4N)$^{3-}$ adopts a rigid conformation due to the insertion of the Me_4N^+ cation into the cavity; for the (Cal, Pr_4N)$^{3-}$ the flexibility of the calixarene is only reduced partially because of the insertion of only one alkyl chain into the cavity.

These simulations allow a better understanding of the contribution of the desolvation in the association process. No desolvation of the sulfonate groups of the calixarene is observed. However, we note that the number of water molecules in the cavity decreases from eight for the free ligand to four for the lanthanide complex and we observe a total cavity desolvation upon complexation of the tetraalkylammonium cations.

The residence times of the water molecules inside the cavity of the free calixarene and of the (Cal, La)$^-$ complex have been successfully calculated. The presence of the guest molecule reduces the exchange process between inside and outside the cavity.

In summary, these simulations establish the simple pair model as an appropriate model to study the structural and energetic features of these complexes. However, it would be interesting to check the contribution of the polarization and charge transfer effects, even if the inclusion of polarization effects in the potential model dramatically complicates the calculations and renders simulations of such complexes cumbersome and time-consuming.

References and Notes

(1) Gutsche, C. D. *Monographs in Supramolecular Chemistry, Calixarenes*; The Royal Society of Chemisrty: London, 1989.
(2) Vicens, J.; Bohmer V. *Calixarenes. A Versatile Class Of Macrocyclic Compounds*; Kluwer Academic: Dordrecht, 1991.
(3) Lehn, J. M.; Meric, R.; Vigeneron, J. P.; Cesario, M.; Guilhem, J.; Pascard, C.; Asfari, Z.; Vicens, J. *Supramol. Chem.* **1995**, *5*, 97.
(4) Atwood, J. L.; Hamada, F.; Robinson, K. D.; Orr, G. W.; Vincent, R. L. *Nature* **1991**, *349*, 683.
(5) Atwood, J. L.; Orr, G. W.; Robinson, K. D.; Hamada, F. *Supramol. Chem.* **1993**, *2*, 309.
(6) Atwood, J. L.; Bott, S. G. *Calixarenes. A Versatile Class of Macrocyclic Compounds;* Vicens, J., Bohmer, V.; Kluwer Academic: Dordrecht, 1991; p 199.
(7) Atwood, J. L.; Coleman, A. W.; Bott, S. G.; Morley, S. D.; Means, C. M.; Robinson, K. D.; Zhang, H. *Angew. Chem. Int. Ed. Engl.* **1988**, *27*, 1361.
(8) Atwood, J. L.; Coleman, A. W.; Zhang, H.; Bott, S. G. *J. Incl. Phenom.* **1989**, *7*, 203.
(9) Bonal, C.; Israeli, Y.; Morel, J.-P.; Morel-Desrosiers N. *J. Chem. Soc., Perkin Trans.* **2001**, *2*, 1075.
(10) Israeli, Y.; Bonal, C.; Detellier, C.; Morel, J. P.; Morel-Desrosiers N. *Can. J. Chem.* **2002**, *80*, 163.
(11) Scharff, J. P.; Mahjoubi, M.; Perrin, R. *New. J. Chem.* **1991**, *15*, 883.
(12) Arena, G.; Cali, R.; Lombardo, G. G.; Rizzarelli, E.; Sciotto, D.; Ungaro, R.; Casnati, A. *Supramol. Chem.* **1992**, *1*, 19.
(13) Yoshida, I.; Yamamoto, N.; Sagara, F.; Ishii, D.; Ueno, D.; Shinkai, S. *Bull. Chem. Soc. Jpn.* **1992**, *65*, 1012.
(14) Atwood, J. L.; Barbour, L. J.; Junk, P. C.; Orr, W. *Supramol. Chem.* **1995**, *5*, 105.
(15) Kowall, Th.; Foglia, F.; Helm, L.; Merbach, A. E *J. Am. Chem. Soc.* **1995**, *117*, 3790.
(16) Mahoney, M. W.; Jorgensen, W. *J. Chem. Phys.* **2000**, *112*, 8910.
(17) Cornell, W. D.; Cieplak, P.; Bayly, C. I.; Gould, I. R.; Merz, K. M., Jr; Ferguson, D. M.; Spellmeyer, D. M.; Fox, T.; Caldwell, J. W.; Kollman, P. *J. Am. Chem. Soc.* **1995**, *117*, 5179.
(18) Ryckaert, J. P.; Ciccotti, G.; Berendsen, H. J. C. *J. Comput. Phys.* **1977**, *23*, 327.
(19) Tobias, D. J.; Klein, M. L. *J. Phys. Chem.* **1996**, *100*, 6637.
(20) Veggel van, F. C. J. M.; Reinhoudt, D. N. *Chem. Eur. J.* **1999**, *4*, 90.
(21) Durand, S.; Dognon, J. P.; Guilbaud, P.; Rabbe, C.; Wipff, G. *J. Chem. Soc., Perkin Trans.* **2000**, *2*, 705.
(22) Selkti, M.; Coleman, A. W.; Nicolis, I., Douteau-Guével, N.; Villain, F.; Tomas, A.; de Rango, C. *Chem. Commun.* **2000**, 161.
(23) Jorgensen, W. L.; Chandrasekhar, J.; Madura, J. D. *J. Chem. Phys.* **1983**, *79*, 926.

(24) Allen, M. P.; Tildesley, D. J. *The Computer Simulation of Liquids;* Clarendon Press: Oxford, 1987.
(25) Berendsen, H. J. C.; Postma, J. P. M.; van Gunsteren, A.; DiNola, A.; Haak, J. R. *J. Chem. Phys.* **1984**, *81*, 3684.
(26) Street, W. B.; Tildesley, D. J.; Saville, G. *Mol. Phys.* **1978**, *35*, 639.
(27) DL_POLY is a parallel molecular dynamics simulation package developed at the Daresbury Laboratory Project for Computer Simulation under the auspices of the EPSRC for the Collaborative Computational Project for Computer Simulation of Condensed Phases (CCP5) and the Advanced Reserach Computing Group (ARCG) at the Daresbury Laboratory.
(28) Zwanzig, R. W. *J. Chem. Phys.* **1954**, *22*, 1420.
(29) Mezei, M.; Beveridge, D. L. *Ann. N.Y. Acad. Sci. U.S.A.* **1986**, *482*, 1.
(30) Pearlman, D. A. *J. Comput. Chem* **1994**, *15*, 105.
(31) Mezei, M.; Swaminathan, S.; Beveridge, D. L. *J. Am. Chem. Soc.* **1978**, *100*, 3255.
(32) Rudnick, J.; Gaspari, G. *Science* **1987**, *237*, 384.
(33) Lee, S. H.; Rasaiah, J. C. *J. Chem. Phys.* **1994**, *101*, 6964.
(34) Lyubartsev, A. P.; Laaksonen A. *J. Phys. Chem.* **1996**, *100*, 16410.
(35) Smith, D. E.; Dang, L. X. *J. Chem. Phys.* **1994**, *100*, 3757.
(36) Impey, R.; Dang, L. X. *J. Chem. Phys.* **1994,** *100*, 3757.
(37) Hawlicka, E.; Swiatla-Wojcik, D. *Phys. Chem. Chem. Phys.* **2000**, *2*, 3175.